Simple traits predict complex temperature responses across scales

Daniel Wieczynski (daniel.wieczynski@gmail.com)
Duke University
Pranav Singla
Duke University
Adrian Doan
Duke University
Alexandra Singleton
Duke University
Zeyi Han
Duke University https://orcid.org/0000-0001-5552-8636
Andrea Yammine
Duke University
Jean Gibert
Duke University https://orcid.org/0000-0002-5083-6418

Article

Keywords: Climate change, Microbial diversity, Community ecology, Temperature, Ecosystem functioning

Posted Date: January 22nd, 2021

DOI: https://doi.org/10.21203/rs.3.rs-116110/v1

TITLE

Simple traits predict complex temperature responses across ecological scales

AUTHORS

Daniel J. Wieczynski[1,*], Pranav Singla[1,2], Adrian Doan[1], Alexandra Singleton[1], Zeyi Han[1], Samantha Votzke[1], Andrea Yammine[1], Jean P. Gibert[1]

AFFILIATIONS

[1] Department of Biology, Duke University, 130 Science Drive, Durham, NC 27708, USA

[2] North Carolina State University, Raleigh, NC, USA

* Corresponding author: daniel.wieczynski@duke.edu

KEYWORDS

Climate change, Microbial diversity, Community ecology, Temperature, Ecosystem functioning

ABSTRACT

Microbial communities regulate ecosystem responses to climate change. But predicting these responses is challenging due to complex interactions among processes at multiple ecological scales. Organismal traits that determine individual performance and ecological interactions are essential for scaling up predictions of environmental responses from individuals to ecosystems. We combine experiments and mathematical models to show that key microbial traits—cell size, shape, and cell contents—independently drive shifts in demographic rates across temperatures, having cascading effects on community structure, dynamics, and ecosystem function. Moreover, intra- and interspecific trait variation play distinct, trait-specific roles in temperature responses. These species-level responses scale up to cause predictable, nonlinear shifts in microbial community composition and respiration rates, with direct implications for the effects of warming on the global carbon cycle. Mechanistically linking microbes with climate using traits will help refine predictions about complex ecosystem-climate feedbacks and the pace of climate change.

INTRODUCTION

Climate regulates the organization, function, and dynamics of ecosystems[1,2], yet predicting ecosystem responses to rapid environmental change remains a major challenge in ecology[3–5]. This is partly due to the complexity of ecological systems—which involve processes at multiple organizational scales, from individuals to ecosystems[6]. Forecasting ecosystem responses to climate change therefore hinges on understanding how novel environmental conditions influence processes at each scale and how these simultaneous responses are linked across scales[2,3,7,8].

The processes that structure populations, communities, and ecosystems are ultimately determined by interactions between individual organisms and their biotic and abiotic environment[6,7]. Traits control these individual-level interactions[9,10] and are thus central to linking processes across scales and predicting complex ecosystem responses to climate change[11–13]. For example, body size controls individual metabolic rates[14], which in turn influence population-level processes like intrinsic growth rates and carrying capacities[15–17]. At the community-level, trait variation within and among species can influence competitive outcomes[18–20] and the strength and occurrence of trophic interactions[20–24]. Finally, through their effects on individual metabolic rates, functional traits like body size can scale up to determine ecosystem-level properties like total biomass, biodiversity, primary productivity, and nutrient cycling[11–13,25,26].

Although traits can link processes across scales[9–13], the challenge is to determine 1) which trait—or combination of traits—is the most important driver of variation for each ecological process and 2) how these traits mediate ecological responses to environmental change across scales. However, linking individual-level traits to changes in ecological processes across scales under different environmental conditions is remarkably challenging for multiple reasons. First, relevant functional traits must be accurately quantified at the individual level. Second, intra- and inter-specific trait variation must be linked to variation in the demographic rates that determine population dynamics, thus linking traits to population-level processes. Third, these responses must then be considered in a community context to evaluate how trait-driven demographic variation affects the composition, structure, and dynamics of communities and their associated ecosystem consequences. Last, all of these patterns—trait-driven shifts in species densities,

73 community structure, and ecosystem functioning—must be characterized across environmental
74 conditions, which is infeasible in most systems[27,28].
75
76 Microbial communities are key drivers of ecosystem responses to climate change[29–31] that also
77 provide an opportunity to study environmental effects across scales comprehensively in
78 controlled laboratory conditions[27,28]. Indeed, microbial decomposers have a significant influence
79 on nutrient flux and the global carbon cycle that ultimately determine the pace of climate
80 change[31,32]. For example, bacteria and fungi store 41 times more carbon than the entire animal
81 kingdom[33] while soil prokaryotic respiration alone releases 98 Pg C yr^{-1} [34], representing one of
82 the largest sources of atmospheric carbon emissions[35] that is expected to rise with global
83 warming[36]. The principal consumers of these microbial decomposers worldwide are a group of
84 single-celled eukaryotes collectively known as protists[37,38], which account for twice as much
85 biomass as the entire animal kingdom globally[33]. Predation by protists depresses microbial
86 biomass, thus controlling total microbial respiration rates and, consequently, global carbon
87 sequestration and nutrient flux[38]. However, it is largely unknown how this important biotic
88 control on global ecosystem functioning may respond to rising temperatures[39]. It is possible to
89 study how traits mediate these microbial interactions across environment gradients in great detail
90 in the laboratory, which provides a unique opportunity to understand the mechanisms connecting
91 ecological processes across scales while informing how ongoing climate change may influence
92 global nutrient cycling.
93
94 Here, we combine laboratory experiments and mathematical modeling to examine how protist
95 traits influence population-, community-, and ecosystem-level responses to temperature. We

study 14 protist species that commonly co-occur in nature[40], span several orders of magnitude in body size, and play a variety of functional roles within microbial communities (producers, bacterivores, detritivores, grazers, intraguild predators)[39,40]. Specifically, we ask: Do protist traits predict population, community, and ecosystem-level responses to changes in temperature? We find that intra- and interspecific variation in three key traits—body size, shape, and cellular contents (Figure 1)—are strongly, but distinctly, related to temperature-driven shifts in species demographic parameters controlling population growth and species interactions. These population-level effects scale up to determine how community- and ecosystem-level properties change across temperatures—including shifts in equilibrium densities, community network structure, species richness, and total system respiration. Our results show how traits link environmental variation to complex ecological responses across scales, thus providing insights into how key microbial components of ecosystems might respond to a rapidly changing climate.

RESULTS

We found remarkable trait diversity both within and among species along three main axes of variation (Figures 1A & 2). Body size spanned over four orders of magnitude across species (Figure 2A) while body shape ranged from fusiform to nearly perfectly spherical (Figure 2B). Cell contrast—which measures the optical homogeneity of a cell and is indicative of cellular contents (vacuoles, organelles, etc.), storage, and consumption—also varied widely (Figure 2C). All traits were quantified prior to experimental manipulations.

Species exhibited distinctive Temperature Performance Curves (TPCs, Figure 1B), indicating a variety of strategies to handle temperature variation (Figures 3A & S1; Table S1). Optimal

119 temperatures for growth (T_{opt}, Figure 1B) spanned over 12ºC across species from 20.4ºC in *C.*
120 *striatum* to 32.3ºC in *T. pyriformis*. The range of viable temperatures (T_{range}, Figure 1B) also
121 varied widely across species from 12.4ºC in *Euplotes sp.* to 24.7ºC in *T. magna*. All TPCs were
122 left-skewed (Figure 3A), but the magnitude of this asymmetry varied from nearly perfect
123 symmetry in *P. aurelia* ($TPC_{asymmetry} \approx 2.0$ºC) to extreme asymmetry in *T. pyriformis*
124 ($TPC_{asymmetry} \approx 19$ºC). Intrinsic growth rate at T_{opt}, or r_{peak} (measured in cells cell^{-1} d^{-1}; Figure 1B)
125 ranged from 0.2 in *P. bursaria* to 4.6 in *T. pyriformis* (Figure 3A). Several relationships among
126 TPC parameters also emerged. Interestingly, r_{peak} was not correlated with T_{opt} itself (Figure S2),
127 nor was it related to any features of the falling parts of TPCs (including CT_{max} or deactivation
128 energy, E_d). Instead, r_{peak} was strongly related to T_{range} ($\rho = 0.53$) and features of the rising parts
129 of TPCs (CT_{min}, $\rho = -0.65$; E_a, $\rho = 0.84$). Conversely, T_{opt} was only correlated with the falling
130 parts of TPCs (CT_{max}, $\rho = 0.89$; E_d, $\rho = 0.57$; $TPC_{asymmetry}$ $\rho = 0.62$). $TPC_{asymmetry}$ was
131 significantly correlated with T_{range} ($\rho = 0.73$), CT_{min} ($\rho = -0.54$), and E_d ($\rho = 0.81$).
132
133 We assessed the density dependence of population growth for each species at two different
134 temperatures—22ºC and 25ºC—by measuring per-capita growth rates across a range of initial
135 population densities, then using the y-intercepts (b) and slopes (m) of these relationships to
136 calculate intrinsic growth rates ($r = b$; in cells cell^{-1} d^{-1}) and carrying capacities ($K = -b/m$; in
137 cells mL^{-1})—important demographic parameters that control population dynamics and
138 community-level interactions (Figure 1C). Density dependence varied among species and was
139 also sensitive to changes in temperature (Figure 3B). Linear models revealed that all species,
140 except *T. pyriformis, U. turbo* and *P. caudatum* (*P. caudatum* was marginally significant at p =
141 0.06), exhibited significant negative density dependence (Table S2). All species showed

142 significant differences in intercepts between temperatures, while four species showed significant
143 differences in slope between temperatures, indicating interacting effects of density and
144 temperature on growth (Figure 3B). Intrinsic growth rates (r) increased with temperature in all
145 but three species (Figure 3B). Estimates of r from density dependence assays agreed with TPC
146 estimates (R^2 = 0.86; Figure 3C). K increased with temperature in five species but decreased in
147 seven other species (Figure 3B). The direction of change (increase or decrease) in K with
148 temperature matches that of r in all species except those that exhibited a significant interaction
149 between density and temperature effects on growth (Figure 3B inset).
150
151 Traits significantly predicted observed properties of TPCs (Figure 4A) and demographic
152 responses to temperature (r & K; Figure 4B). Species with larger size had lower peak intrinsic
153 growth rates (r_{peak}) and higher critical thermal minima (CT_{min}). More symmetrically-shaped
154 (higher aspect ratio) species had higher r_{peak}, lower CT_{min}, and wider thermal breadths (T_{range}).
155 Cell contrast was positively related to r_{peak} and activation energy (E_a). Interestingly, no trait
156 mean significantly predicted T_{opt}, $TPC_{asymmetry}$, CT_{max}, or E_d (Figure S2). The observed decrease
157 in r estimates (from density-dependence assays) with cell size was consistent with predictions
158 from metabolic theory (expected slope ≈ -0.25)[14,15], but did not significantly differ across
159 temperatures (m_{22} = -0.28, m_{25} = -0.21). r also increased with cell aspect ratio at both
160 temperatures (22ºC and 25ºC). While not related to size or shape, the steepness of the rising part
161 of the TPCs (represented by r_{diff} and E_a) was positively related to cell contrast. Carrying capacity
162 (K) declined with increasing size and was not related to any other traits. While this negative K-
163 size trend is consistent with theory, the slopes did not vary with temperature (m_{22} = -0.42, m_{25} = -
164 0.41) and were not close to the expected value of -0.75[14,15,17]. However, the magnitude of the

difference in K between temperatures (K_{diff}) declined with size, indicating that larger species with lower Ks also experience smaller changes in K with temperature. Although r_{peak}, r_{22}, r_{25}, and CT_{min} were all related to multiple traits, commonality analysis revealed that metrics of r were more strongly influenced by body shape, while CT_{min} was more strongly influenced by body size (Table S3).

Intraspecific variation in traits also predicted demographic parameters (Figure S2). Variance in cell volume and contrast were significantly correlated with r_{peak}. Variance in cell contrast predicted many demographic parameters that were not related to mean contrast like intrinsic growth rate (r_{22}, r_{25}), carrying capacity (K_{22}, K_{25}, K_{diff}), and different TPC components (CT_{min}, T_{range}, $TPC_{asymmetry}$). Variance in contrast and mean volume were the only trait variables related to carrying capacity (K). Variance in contrast was the only trait variable that predicted $TPC_{asymmetry}$.

A mathematical model parameterized with our TPC data (details in Methods) showed that observed trait-mediated differences in species' demographic responses to changes in temperature should lead to predictable changes in population-, community- and ecosystem-level properties across temperatures (Figure 5). Species' realized thermal niches varied according to a combination of species' thermal ranges (fundamental niches) and interactions with other species with overlapping thermal ranges (Figure 5A). Changes in temperature caused coordinated shifts in species equilibrium densities and ecological interactions via changes in r along TPCs. As a result, our model shows that temperature should alter community composition, and the topology of interaction networks, in predictable ways (shown as network diagrams in Figure 5A). Increasing the strength of competitive differences among species (by increasing background

mortality δ, Eqn. 4) led to lower equilibrium densities and species exclusions, generally favoring faster growing species (i.e., species with higher r_{peak} values). The most dramatic changes in equilibrium densities and community structure occurred at intermediate levels of competition (Figure 5A).

Our trait-driven community model also predicted shifts in community composition associated with nonlinear changes in species richness, mean species mass, and whole community respiration across temperatures (Figure 5 B–D). Intermediate temperatures (~20–25°C) hosted the most diverse communities and declines in diversity at extreme temperatures mirrored asymmetry in TPCs (Figure 5B). In contrast, mean species mass tended to increase with temperature, owing to shifts in species composition favoring larger species at warmer temperatures (Figure 5C). Coordinated shifts in equilibrium densities and mean species mass produced a complex relationship between temperature and total protist community respiration rate—an indicator of overall bacterial consumption[41]—that showed quantitative differences with that of species richness (Figure 5D). While patterns in respiration rate also were generally hump-shaped, they showed less sensitivity to increases in the strength of competition than species richness, indicating that metabolic losses from competitive species exclusions were likely compensated by changes in the mass-densities of remaining species (Figure 5 B–D). As with richness, however, respiration is predicted to peak at intermediate temperatures, although overall temperature dependence is right-shifted and declines at a lower rate at high temperatures compared to species richness, coinciding with the high-temperature peak in mean species mass (Figure 5C), and contrasting with a sharp decline in species richness (Figure 5B).

Interestingly, our results from empirical communities support all of these predictions: 1) we observed a hump-shaped relationship between richness and temperature, peaking at levels consistent with model predictions (Figure 5E), 2) empirical communities increased in mean species mass with temperature, in striking agreement with model predictions (Figure 5F), and 3) observed changes in species richness and mean species mass produced a hump-shaped relationship between respiration rate and temperature that declines at a lower rate than species richness does at high temperatures (Figure 5G). We note, however, that empirical estimates of respiration are roughly 20x higher than theoretical respiration rates, likely owing to additional respiration by bacteria in experimental microcosms. Taken together, these results affirm that directly linking environmental conditions to population and community processes using traits can greatly improve our understanding and predictions of changes in species richness and total respiration rate across temperatures.

DISCUSSION

Our results suggest that future warming will cause complex, coordinated shifts in microbial community composition and respiration, having significant impacts on ecosystem functioning that can be predicted by individual-level traits. Indeed, disentangling the unique roles of specific microbial traits on species' demographic responses to temperature (Figures 4 & S2; Table S3), allows us to mechanistically track how temperature drives shifts in species richness, community network structure, and total community respiration (Figure 5). As the 'puppet masters' of microbial communities, protists play an integral role in the global carbon cycle through their strong top-down control of microbial community structure, respiration, and nutrient flux[38]. By mechanistically linking environmental variation with microbial processes across scales through

234 protist traits, our framework opens up possibilities to create a more holistic understanding of
235 climate-ecosystem feedbacks. Such a multi-level, multi-trait approach is crucial for explaining
236 spatiotemporal variation in the structure and function of ecosystems and forecasting complex
237 ecological responses to climate change[11–13].
238
239 Consistent with metabolic theory[14,15], protist intrinsic growth rates declined significantly with
240 increasing body size across temperatures. However, our analysis suggests that body shape may
241 actually be a stronger predictor of intrinsic growth rates (r_{22}, r_{25}, and r_{peak}) than body size in
242 protists (Table S3, Figure S2). This shows how multiple traits can have important but distinct
243 effects on higher-level processes. Why cell shape would influence demographic parameters is
244 poorly understood, but has been observed at least once before[42]. Because body shape determines
245 the surface area to volume ratio in unicellular organisms, it mediates the rate of passage of
246 material across the cell membrane[41]. On the other hand, cell size determines metabolic costs[14].
247 Since body size and shape were not correlated in our data, it is possible that both traits jointly
248 regulate metabolic rate, but do so independently: size sets energetic demands while surface sets
249 energetic intake[43,44]. More generally, these results suggest that traits other than size may play a
250 significant role in determining ecological effects across scales, as recently shown in multicellular
251 organisms like cephalopods[45] and birds[46].
252
253 Both inter- and intraspecific variation have been shown to influence ecological processes[9,20], but
254 how these mediate temperature responses is less clear. Our results show that trait variation across
255 species (mean trait values) and within species (trait variances) are both important but
256 independent predictors of population growth across temperatures (Figure S2). Indeed, r_{peak} was

the only parameter related to both trait mean and variance (in both cell volume and contrast)—all other significant trait-demography relationships involved either trait mean or variance, but not both. This suggests that intra- and inter-specific trait variation play distinct, trait-specific roles within ecosystems. Identifying these unique roles will help clarify which aspects of functional diversity are most important in mediating temperature effects on higher-level processes, thus informing predictions about the cascading ecosystem effects of biodiversity shifts with future climate change.

Species trait distributions are likely to shift in response to environmental change through plasticity or rapid evolution[47]. This could, in turn, alter how population, community, and ecosystem responses develop over longer periods of time. For example, body size declines with increasing temperature—a pattern known as the 'temperature-size rule'[48]. It is unclear whether such shifts in body size will amplify or compensate for temperature effects across levels of organization, especially if the temperature-size rule varies among species[49]. To fully understand how plastic or evolutionary change may mediate climate responses across levels of biological organization, we might need to incorporate an eco-evolutionary perspective in our current predictive models[50]. Because traits govern population, community and ecosystem processes[11–13] (Figures 4 & 5) while also influencing fitness and being subject to selection[20], they provide a natural link between ecology and evolution. Our results represent the first step in that direction by showing that even small temperature differences can lead to profound effects across scales, and that these responses can be predicted by traits.

Because microbes are key players in global climate responses, understanding how they will collectively respond to changes in environmental conditions is a crucial goal[29–31]. In our system, we identified traits that predict protist's temperature responses (TPCs), leading to coordinated changes in equilibrium densities, community body size distributions, and, ultimately, total community respiration rates (through increased metabolic rates) across temperatures. As a result, our model predicts that rapid warming will produce nonlinear shifts in carbon flux via complex but predictable changes in protist communities and overall consumption of decomposers, driven by changes in protist metabolic demands (Figure 5). Most current earth systems models (ESMs) treat microbial respiration as a black box, assuming that total microbial respiration increases with temperature[51,52]. Here, we link respiration to the individual traits that determine functional composition and dynamics of microbial communities, thus providing a more comprehensive and mechanistic approach that can be used to improve model predictions (e.g., from ESMs) of ecosystem responses to environmental change.

METHODS

Laboratory experiments

Species cultures

We studied 14 protist species across functional groups (by increasing r_{peak} value): *Paramecium bursaria* (myxotroph), *Paramecium multimicronucleatum* (grazer, bacterivore), *Euplotes sp.* (bacterivore, intraguild predator), *Blepharisma sp.* (bacterivore, intraguild predator), *Colpidium striatum* (grazer, bacterivore), *Paramecium aurelia* (grazer, bacterivore), *Paramecium caudatum* (grazer, bacterivore), *Tillina magna* (grazer, bacterivore), *Halteria grandinella* (bacterivore), *Cyclidium glaucoma* (bacterivore), *Colpoda steinii* (bacterivore), *Glaucoma sp.* (bacterivore),

and *Tetrahymena pyriformis* (bacterivore). Stock cultures of all species were maintained in 200mL jars at 22ºC in Carolina protist media with 1 wheat seed as a carbon source[27].

Trait measurements

All traits (cell volume, aspect ratio, and optical contrast) were measured using fluid imaging (FlowCam, Portland, ME). One mL samples were taken from stock cultures for each species and imaged at 10x magnification to create libraries of images of individual cells. Cell volume was calculated as the volume of a prolate spheroid based on the geodesic width (a) and geodesic length (b) measurements of each cell ($biomass = 4/3\pi a^2 b$). Cell aspect ratio was calculated as the ratio of geodesic width to length ($aspect\ ratio = a/b$, Figure 1A). The FlowCam proprietary software erroneously characterized some cells as perfect spheres ($aspect\ ratio = 1$, Figure 1B); those samples were not used for data analysis. Cell contrast was measured as the standard deviation of grayscale values for each individual cell image (Figure 1A). For *Euplotes sp.* and *T. magna*, 10x samples were used for biomass and aspect ratio measurements while separate samples were processed at 4x to more reliably quantify cell contrast. Trait estimates were $\log_{10}$-transformed and all estimates within three standard deviations of the $\log_{10}$-transformed mean (geometric mean) for each species-trait combination were used for analysis.

Experimental design

Thermal performance curve (TPC) assays. TPCs were characterized using the standard approach[53,54], i.e., by quantifying intrinsic population growth rates ($r = log(Final\ density/Initial\ density)/days$) across temperatures (replication: n=6/temperature, 5 temperatures/species, see online Dataset). Each replicate population was grown for three days, beginning at an initial

density ($N_{initial}$) of three individual cells taken from stock cultures (due to their small size, *C. glaucoma* replicates were initialized by volume of 20µL (average density of 2.28 inds. μL^{-1}) rather than transferring individual cells. TPCs fits were then estimated using nonlinear regression of a Sharpe-Schoolfield model[55] ('nls.multstart' package[56] in R[57]) to empirical *r* values across temperatures (ln-transformed here):

$$ln(r) = a + \frac{E_a}{k}\left(\frac{1}{T_r} - \frac{1}{T}\right) - ln\left(1 + e^{\frac{E_d}{k}\left(\frac{1}{T_h} - \frac{1}{T}\right)}\right) \quad \text{Equation (1)}$$

where *r* is intrinsic growth rate, *a* is a normalization constant, E_a is activation energy, *k* is Boltzmann's constant ($8.6*10^{-5}$ eV/K), T_r is a reference temperature (T_r = 25ºC), *T* is temperature, E_d is deactivation energy, and T_h is the temperature to the right of T_{opt} where *r* is half of r_{peak}. T_{opt} can be calculated from the above parameters as:

$$T_{opt} = E_d \frac{T_h}{E_d + kT_h ln\left(\frac{E_d}{E_a} - 1\right)} \quad \text{Equation (2)}$$

To account for negative *r* values and avoid the lower asymptote of the Sharpe-Schoolfield model interfering with fits, a scaling coefficient (*S* = 10) was added to all *r* values ($r = r_{raw}+S$) prior to fitting and removed after fitting.

Density-dependence (DD) assays. Temperature effects on density dependence were quantified by calculating intrinsic population growth rates (*r*) for four replicate populations of each species at 22ºC and 25ºC across a range of increasing initial densities—$N_{initial}$ = 4, 8, 12, 16, & 20 cells. As in TPC assays, *C. glaucoma* replicates were initialized by increasing volumes (10, 40, 60, 100, 140, 200µL) of known densities (average density of 3.13 inds. μL^{-1}). Each replicate grew for two days (except *T. pyriformis* populations which were sampled after 10hrs due to extremely fast

growth) and final densities and *r* were measured as in TPC assays. *r* estimates within three standard deviations of the mean for each species-temperature combination were used for analysis. Effects of initial density ($N_{initial}$), temperature (T), and interactions between initial density and temperature ($N_{initial}*T$) on per-capita population growth rate were analyzed using a linear model:

$$Growth\ rate = N_{initial} + T + N_{initial} * T + \text{error} \quad \text{Equation (3)}$$

For each species, we compared models with and without the interaction term, and whenever interaction terms were significant, the model containing the interaction was kept for further analysis. Otherwise, the main effects model was used. Table S2 provides a model summary including model choices, model p-values, variable coefficient estimates (β), variable standard errors, and variable p-values.

Demographic parameters

To quantify changes in population growth across temperatures we calculated 14 demographic parameters based on TPC and DD assays:

Demographic Parameter	**Abbr.**
peak intrinsic growth rate	r_{peak}
optimal temperature	T_{opt}
critical minimum temperature	CT_{min}
critical maximum temperature	CT_{max}
thermal breadth	T_{range}
TPC asymmetry	$TPC_{asymmetry}$
activation energy	E_a
deactivation energy	E_d
r at 22ºC	r_{22}
r at 25ºC	r_{25}

magnitude of change in r from 22ºC to 25ºC	$\lvert r_{diff} \rvert$
K at 22ºC	K_{22}
K at 22ºC	K_{25}
magnitude of change in K from 22ºC to 25ºC	$\lvert K_{diff} \rvert$

All TPC parameters (r_{peak}, T_{opt}, CT_{min}, CT_{max}, T_{range}, $TPC_{asymmetry}$, E_a, and E_d) were recorded from Sharpe-Schoolfield fits of raw intrinsic growth rate data (Figure 1A). DD parameters (intrinsic growth rate (r, in cells cell^{-1} d^{-1}) and carrying capacity (K, in cells mL^{-1})) were calculated for each temperature (22ºC and 25ºC) using y-intercepts (b) and slopes (m) from linear models (Table S2) as $r = b$ and $K = -b/m$. The magnitudes of changes in r and K were calculated as the absolute value of the difference between values at each individual temperature ($|r_{diff}| = |r_{25}-r_{22}|$; $|K_{diff}| = |K_{25}-K_{22}|$). Resulting demographic parameters were $\log_{10}$-transformed prior to analysis.

Demographic parameter-trait analyses

Relationships between demographic parameters and traits were evaluated using a combination of correlation analysis, linear models, and commonality analysis[58]. For each species, mean and variance of log-transformed trait values were used for comparison with demographic parameters. Because the focal temperatures of density dependence assays (22ºC and 25ºC) occur to the left of T_{opt} for all species except *C. striatum*, all density dependence parameters (r and K) for *C. striatum* were omitted in demographic parameter-trait analyses. Because the $N_{initial}$ effects in density dependence models were not significant for *U. turbo* or *T. pyriformis*, K estimates for these species were omitted from these analyses.

Pearson correlation coefficients (ρ) and associated p-values were calculated for all demographic parameter-trait moment combinations (Figure S2). Linear regressions were also performed for all

combinations of demographic parameters and mean traits (significant results shown in Figure 4). For demographic parameters related to multiple traits, we performed a commonality analysis[58] using the 'yhat' package[59] in R to partition the total explained variance (R^2) into the individual contributions of each trait (U). Predictor variables (traits) were centered and rescaled prior to doing commonality analysis to standardize the scales of their effects—note that this rescaling does not affect variance partitioning. Results of the commonality analysis are summarized in Table S3, including total explained variance (R^2) model p-values, the main effects of each trait (β), variance inflation factors (VIFs, which describe the degree to which the variance explained by individual traits is inflated by multicollinearity), the proportion of total R^2 that is unique to each trait (U; shown with percentage of R^2 explained (U%)), variance explained that is common between a given trait and all other traits in the model (C), and the total explained variance based on the unique and common effects of each trait (U + C = Total).

Community experiment

Microcosm communities were initialized with 10 protist species (excluding *C. steinii*, *U. turbo*, and predatory species *Euplotes sp.* and *Blepharisma sp.*) at initial densities of 50 inds. mL^{-1} (except *T. magna* which was started at the lower densities of 0.015ind/mL) in 200mL glass jars and for five different temperature treatments: 15, 20, 25, 30 and 35 ºC. Each temperature treatment was replicated 8 times. After 14 days, we estimated species presence/absence and species richness through species counts under a Leica DM2500 stereomicroscopes in 1mL samples, in triplicate. Whole community respiration rates were estimated using an optode-based, closed-system, real-time OXY-4 ST respirometer (PreSens, Regensburg, Germany) for 3 experimental replicate microcosms per temperature. Respiration rate was quantified as the

volume of dissolved O_2 (mL) consumed per mL per second by the entire 200mL microcosm for 25 minutes, relative to a control[60]. Oxygen consumption ($mLO_2\ mL^{-1}\ s^{-1}$) was converted to watts mL^{-1} using a conversion factor of 20J (W*s) per mL of O_2[61]. Respirometry was done in the dark at each experimental temperature, so acclimation times were short (~10 min).

Model of community dynamics

Following previous theory[62,63] and recent advances in microbial ecology[64], community dynamics for all 14 species were analyzed by parameterizing a modified Lotka-Volterra model:

$$\frac{dN_i}{dt} = r_i[T]N_i\left(1 - \frac{N_i}{K_i} - \sum_{j \neq i}\frac{\alpha_{ij}N_j}{K_i}\right) - \delta N_i \qquad \text{Equation (4)}$$

where $r_i[T]$ is the intrinsic growth rate for species i which is a function of temperature (T) according to that species' TPC, N_i (N_j) is the density of species i (j), K_i is the carrying capacity of species i, α_{ij} is the effect of species j on species i, and δ is a global mortality rate[62,63]. For simplicity, all interaction coefficients (α_{ij}) were set to 0.01. Carrying capacities were set to empirically observed values at 22ºC. We relax assumptions about α_{ij} and K_i in Supplementary Figure S3.

At steady-state, equilibrium densities ($\widehat{N}_i$) are:

$$\widehat{N}_i = K_i - \sum_{j \neq i}\alpha_{ij}N_j - \frac{\delta}{r_i[T]} \qquad \text{Equation (5)}$$

Equation (5) shows that, in addition to K_i and α_{ij}, equilibrium densities also depend on r and δ. In order for species to persist, they must be able to invade when rare[65]. Thus, the conditions for species persistence within a community are found by solving Equation (4) such that the per-

capita growth rate of a focal species $\left(\frac{dN_i}{dt}\frac{1}{N_i}\right)$ is greater than zero when rare ($N_i \sim 0$) and all N_j are at their equilibrium densities ($\widehat{N}_j$) in the absence of N_i:

$$\frac{dN_i}{dt}\frac{1}{N_i} = r_i[T]\left(1 - \sum_{j \neq i}\frac{\alpha_{ij}\widehat{N}_j}{K_i}\right) - \delta > 0 \Longrightarrow r_i[T] > \frac{\delta K_i}{K_i - \sum_{j \neq i}\alpha_{ij}\widehat{N}_j} \quad \text{Equation (6)}$$

For a single species in isolation (i.e., all $N_j = 0$), the condition for persistence is:

$$\frac{dN_i}{dt}\frac{1}{N_i} = r_i[T] - \delta > 0 \Longrightarrow r_i[T] > \delta \quad \text{Equation (7)}$$

Here, we calculated equilibrium densities for all species across temperatures (7ºC–41ºC) and global mortality rates (δ= [0.01, 1]). For each of these communities, we also calculated species richness (# of species persisting at equilibrium), mean species mass (average mass across species, in g; using a conversion factor of 10^{-12} g/μm^3), and total community respiration rate (B; in watts mL^{-1}), which is equal to the sum of the metabolic rates of all organisms[66]:

$$B = \sum_{i=1}^{n} W_i\widehat{N}_i \quad \text{Equation (8)}$$

where n is the number of viable species, $\widehat{N}_i$ is the equilibrium density of species i, and W_i is the metabolic rate of species i. Because the temperature dependence of metabolic rate is known to vary among organisms[67] and we did not measure this temperature dependence directly here, we consider the mass effect on metabolic rate combined with the temperature effects on population growth, community composition, and community equilibrium densities studied here. Metabolic rate is proportional to mass:

$$W_i \propto \beta_0 M^{\alpha} \quad \text{Equation (9)}$$

where we use the normalization constant $\beta = 0.00152$ and scaling exponent $\alpha = 0.97$ for protists[68].

DATA AVAILABILITY

All raw and processed data used in this study are available on GitHub https://github.com/JPGibert/protist_temperature_scales (upon publication).

CODE AVAILABILITY

All custom scripts used in this study are available on GitHub https://github.com/JPGibert/protist_temperature_scales (upon publication).

REFERENCES

1. Pachauri, R. K. et al. Climate Change 2014: Synthesis Report. Contribution of Working Groups I, II and III to the Fifth Assessment Report of the Intergovernmental Panel on Climate Change. EPIC3Geneva, Switzerland, IPCC, 151 p., pp. 151, ISBN: 978-92-9169-143-2 151 (IPCC, 2014).
2. Malhi, Y. et al. Climate change and ecosystems: threats, opportunities and solutions. Philos. Trans. R. Soc. B Biol. Sci. **375**, 20190104 (2020).
3. Russell, B. D. et al. Predicting ecosystem shifts requires new approaches that integrate the effects of climate change across entire systems. Biol. Lett. **8**, 164–166 (2012).
4. Clark, J. S. et al. Ecological Forecasts: An Emerging Imperative. Science **293**, 657–660 (2001).

5. Petchey, O. L. et al. The ecological forecast horizon, and examples of its uses and determinants. Ecol. Lett. **18**, 597–611 (2015).
6. Guimarães, P. R. The Structure of Ecological Networks Across Levels of Organization. Annu. Rev. Ecol. Evol. Syst. **51**, 433–460 (2020).
7. Walther, G.-R. Community and ecosystem responses to recent climate change. Philos. Trans. R. Soc. B Biol. Sci. **365**, 2019–2024 (2010).
8. Montoya, J. M. & Raffaelli, D. Climate change, biotic interactions and ecosystem services. Philos. Trans. R. Soc. B Biol. Sci. **365**, 2013–2018 (2010).
9. McGill, B. J., Enquist, B. J., Weiher, E. & Westoby, M. Rebuilding community ecology from functional traits. Trends Ecol. Evol. **21**, 178–185 (2006).
10. Violle, C. et al. Let the concept of trait be functional! Oikos **116**, 882–892 (2007).
11. Enquist, B. J. et al. Chapter Nine - Scaling from Traits to Ecosystems: Developing a General Trait Driver Theory via Integrating Trait-Based and Metabolic Scaling Theories. in Advances in Ecological Research (eds. Pawar, S., Woodward, G. & Dell, A. I.) vol. 52 249–318 (Academic Press, 2015).
12. Gibert, J. P., Dell, A. I., DeLong, J. P. & Pawar, S. Chapter One - Scaling-up Trait Variation from Individuals to Ecosystems. in Advances in Ecological Research (eds. Pawar, S., Woodward, G. & Dell, A. I.) vol. 52 1–17 (Academic Press, 2015).
13. Moran, E. V., Hartig, F. & Bell, D. M. Intraspecific trait variation across scales: implications for understanding global change responses. Glob. Change Biol. **22**, 137–150 (2016).
14. Brown, J. H., Gillooly, J. F., Allen, A. P., Savage, V. M. & West, G. B. Toward a Metabolic Theory of Ecology. Ecology **85**, 1771–1789 (2004).

15. Savage, V. M., Gillooly, J. F., Brown, J. H., West, G. B. & Charnov, E. L. Effects of Body Size and Temperature on Population Growth. Am. Nat. **163**, 429–441 (2004).
16. White, E. P., Ernest, S. K. M., Kerkhoff, A. J. & Enquist, B. J. Relationships between body size and abundance in ecology. Trends Ecol. Evol. **22**, 323–330 (2007).
17. Damuth, J. Population density and body size in mammals. Nature **290**, 699–700 (1981).
18. Kraft, N. J. B., Godoy, O. & Levine, J. M. Plant functional traits and the multidimensional nature of species coexistence. Proc. Natl. Acad. Sci. **112**, 797–802 (2015).
19. Adler, P. B., Fajardo, A., Kleinhesselink, A. R. & Kraft, N. J. B. Trait-based tests of coexistence mechanisms. Ecol. Lett. **16**, 1294–1306 (2013).
20. Bolnick, D. I. et al. Why intraspecific trait variation matters in community ecology. Trends Ecol. Evol. **26**, 183–192 (2011).
21. Schreiber, S. J., Bürger, R. & Bolnick, D. I. The community effects of phenotypic and genetic variation within a predator population. Ecology **92**, 1582–1593 (2011).
22. Barbour, M. A. et al. Genetic specificity of a plant–insect food web: Implications for linking genetic variation to network complexity. Proc. Natl. Acad. Sci. **113**, 2128–2133 (2016).
23. Gibert, J. P. & DeLong, J. P. Phenotypic variation explains food web structural patterns. Proc. Natl. Acad. Sci. **114**, 11187–11192 (2017).
24. Gibert, J. P. & Brassil, C. E. Individual phenotypic variation reduces interaction strengths in a consumer–resource system. Ecol. Evol. **4**, 3703–3713 (2014).
25. Violle, C., Reich, P. B., Pacala, S. W., Enquist, B. J. & Kattge, J. The emergence and promise of functional biogeography. Proc. Natl. Acad. Sci. **111**, 13690–13696 (2014).
26. Wieczynski, D. J. et al. Climate shapes and shifts functional biodiversity in forests worldwide. Proc. Natl. Acad. Sci. **116**, 587–592 (2019).

27. Altermatt, F. et al. Big answers from small worlds: a user's guide for protist microcosms as a model system in ecology and evolution. Methods Ecol. Evol. **6**, 218–231 (2015).
28. Drake, J. A., Huxel, G. R. & Hewitt, C. L. Microcosms as Models for Generating and Testing Community Theory. Ecology **77**, 670–677 (1996).
29. Rustad, L. E., Huntington, T. G. & Boone, R. D. Controls on soil respiration: Implications for climate change. Biogeochemistry **48**, 1–6 (2000).
30. Crowther, T. W. et al. Biotic interactions mediate soil microbial feedbacks to climate change. Proc. Natl. Acad. Sci. **112**, 7033–7038 (2015).
31. Bardgett, R. D., Freeman, C. & Ostle, N. J. Microbial contributions to climate change through carbon cycle feedbacks. ISME J. **2**, 805–814 (2008).
32. Zhou, J. et al. Microbial mediation of carbon-cycle feedbacks to climate warming. Nat. Clim. Change **2**, 106–110 (2012).
33. Bar-On, Y. M., Phillips, R. & Milo, R. The biomass distribution on Earth. Proc. Natl. Acad. Sci. U. S. A. **115**, 6506–6511 (2018).
34. Bond-Lamberty, B. & Thomson, A. Temperature-associated increases in the global soil respiration record. Nature **464**, 579–582 (2010).
35. Friedlingstein, P. et al. Global Carbon Budget 2019. Earth Syst. Sci. Data **11**, 1783–1838 (2019).
36. Smith, T. P. et al. Community-level respiration of prokaryotic microbes may rise with global warming. Nat. Commun. **10**, 5124 (2019).
37. Oliverio, A. M. et al. The global-scale distributions of soil protists and their contributions to belowground systems. Sci. Adv. **6**, eaax8787 (2020).

38. Gao, Z., Karlsson, I., Geisen, S., Kowalchuk, G. & Jousset, A. Protists: Puppet Masters of the Rhizosphere Microbiome. Trends Plant Sci. **24**, 165–176 (2019).
39. Petchey, O. L., McPhearson, P. T., Casey, T. M. & Morin, P. J. Environmental warming alters food-web structure and ecosystem function. Nature **402**, 69–72 (1999).
40. Foissner, W. & Berger, H. A user-friendly guide to the ciliates (Protozoa, Ciliophora) commonly used by hydrobiologists as bioindicators in rivers, lakes, and waste waters, with notes on their ecology. Freshw. Biol. **35**, 375–482 (1996).
41. Fenchel, T. Respiration in aquatic protists. Respir. Aquat. Ecosyst. 47–56 (2004).
42. Gibert, J. P., Allen, R. L., Hruska, R. J. & DeLong, J. P. The ecological consequences of environmentally induced phenotypic changes. Ecol. Lett. **20**, 997–1003 (2017).
43. Hirst, A. G., Glazier, D. S. & Atkinson, D. Body shape shifting during growth permits tests that distinguish between competing geometric theories of metabolic scaling. Ecol. Lett. **17**, 1274–1281 (2014).
44. Glazier, D. S., Hirst, A. G. & Atkinson, D. Shape shifting predicts ontogenetic changes in metabolic scaling in diverse aquatic invertebrates. Proc. R. Soc. B Biol. Sci. **282**, 20142302 (2015).
45. Tan, H., Hirst, A. G., Glazier, D. S. & Atkinson, D. Ecological pressures and the contrasting scaling of metabolism and body shape in coexisting taxa: cephalopods versus teleost fish. Philos. Trans. R. Soc. B Biol. Sci. **374**, 20180543 (2019).
46. Pigot, A. L. et al. Macroevolutionary convergence connects morphological form to ecological function in birds. Nat. Ecol. Evol. **4**, 230–239 (2020).
47. Catullo, R. A., Llewelyn, J., Phillips, B. L. & Moritz, C. C. The Potential for Rapid Evolution under Anthropogenic Climate Change. Curr. Biol. **29**, R996–R1007 (2019).

48. Atkinson, D. Temperature and Organism Size—A Biological Law for Ectotherms? in Advances in Ecological Research (eds. Begon, M. & Fitter, A. H.) vol. 25 1–58 (Academic Press, 1994).
49. Bernhardt, J. R., Sunday, J. M. & O'Connor, M. I. Metabolic Theory and the Temperature-Size Rule Explain the Temperature Dependence of Population Carrying Capacity. Am. Nat. **192**, 687–697 (2018).
50. Kopp, M. & Matuszewski, S. Rapid evolution of quantitative traits: theoretical perspectives. Evol. Appl. **7**, 169–191 (2014).
51. Sulman, B. N., Phillips, R. P., Oishi, A. C., Shevliakova, E. & Pacala, S. W. Microbe-driven turnover offsets mineral-mediated storage of soil carbon under elevated CO 2. Nat. Clim. Change **4**, 1099–1102 (2014).
52. Wieder, W. R. et al. Explicitly representing soil microbial processes in Earth system models. Glob. Biogeochem. Cycles **29**, 1782–1800 (2015).
53. García, F. C., Bestion, E., Warfield, R. & Yvon-Durocher, G. Changes in temperature alter the relationship between biodiversity and ecosystem functioning. Proc. Natl. Acad. Sci. **115**, 10989–10994 (2018).
54. Padfield, D., Yvon-Durocher, G., Buckling, A., Jennings, S. & Yvon-Durocher, G. Rapid evolution of metabolic traits explains thermal adaptation in phytoplankton. Ecol. Lett. **19**, 133–142 (2016).
55. Schoolfield, R. M., Sharpe, P. J. H. & Magnuson, C. E. Non-linear regression of biological temperature-dependent rate models based on absolute reaction-rate theory. J. Theor. Biol. **88**, 719–731 (1981).

56. Padfield, D. & Matheson, G. nls.multstart: Robust Non-Linear Regression using AIC Scores. R package version 1.0.0. (2018).
57. R Core Team. R: A language and environment for statistical computing. (2020).
58. Ray-Mukherjee, J. et al. Using commonality analysis in multiple regressions: a tool to decompose regression effects in the face of multicollinearity. Methods Ecol. Evol. **5**, 320–328 (2014).
59. Nimon, K., Oswald, F. & Roberts, K. Interpreting regression effects. R package version 2.0-0. (2013).
60. Tomlinson, S. et al. Measuring metabolic rates of small terrestrial organisms by fluorescence-based closed-system respirometry. J. Exp. Biol. **221**, (2018).
61. Makarieva, A. M. et al. Mean mass-specific metabolic rates are strikingly similar across life's major domains: Evidence for life's metabolic optimum. Proc. Natl. Acad. Sci. **105**, 16994–16999 (2008).
62. Abreu, C. I., Friedman, J., Andersen Woltz, V. L. & Gore, J. Mortality causes universal changes in microbial community composition. Nat. Commun. **10**, 2120 (2019).
63. Abrams, P. A. Density-Independent Mortality and Interspecific Competition: A Test of Pianka's Niche Overlap Hypothesis. Am. Nat. **111**, 539–552 (1977).
64. Lax, S., Abreu, C. I. & Gore, J. Higher temperatures generically favour slower-growing bacterial species in multispecies communities. Nat. Ecol. Evol. **4**, 560–567 (2020).
65. Grainger, T. N., Levine, J. M. & Gilbert, B. The Invasion Criterion: A Common Currency for Ecological Research. Trends Ecol. Evol. **34**, 925–935 (2019).
66. Enquist, B. J. et al. Scaling metabolism from organisms to ecosystems. Nature **423**, 639–642 (2003).

67. Dell, A. I., Pawar, S. & Savage, V. M. Systematic variation in the temperature dependence of physiological and ecological traits. Proc. Natl. Acad. Sci. U. S. A. **108**, 10591–10596 (2011).
68. DeLong, J. P., Okie, J. G., Moses, M. E., Sibly, R. M. & Brown, J. H. Shifts in metabolic scaling, production, and efficiency across major evolutionary transitions of life. Proc. Natl. Acad. Sci. **107**, 12941–12945 (2010).

ACKNOWLEDGMENTS

This work was supported by the U.S. Department of Energy, Office of Science, Office of Biological and Environmental Research, Genomic Science Program under Award Number DE-SC0020362.

AUTHOR CONTRIBUTIONS

DJW, PS, AY, and JPG designed the study. AY and JPG designed the experiments. All authors collected data for this project. DJW performed all mathematical modeling and DJW and JPG analyzed the data. DJW wrote the first version of the manuscript and all authors contributed to subsequent versions.

618 **FIGURES**

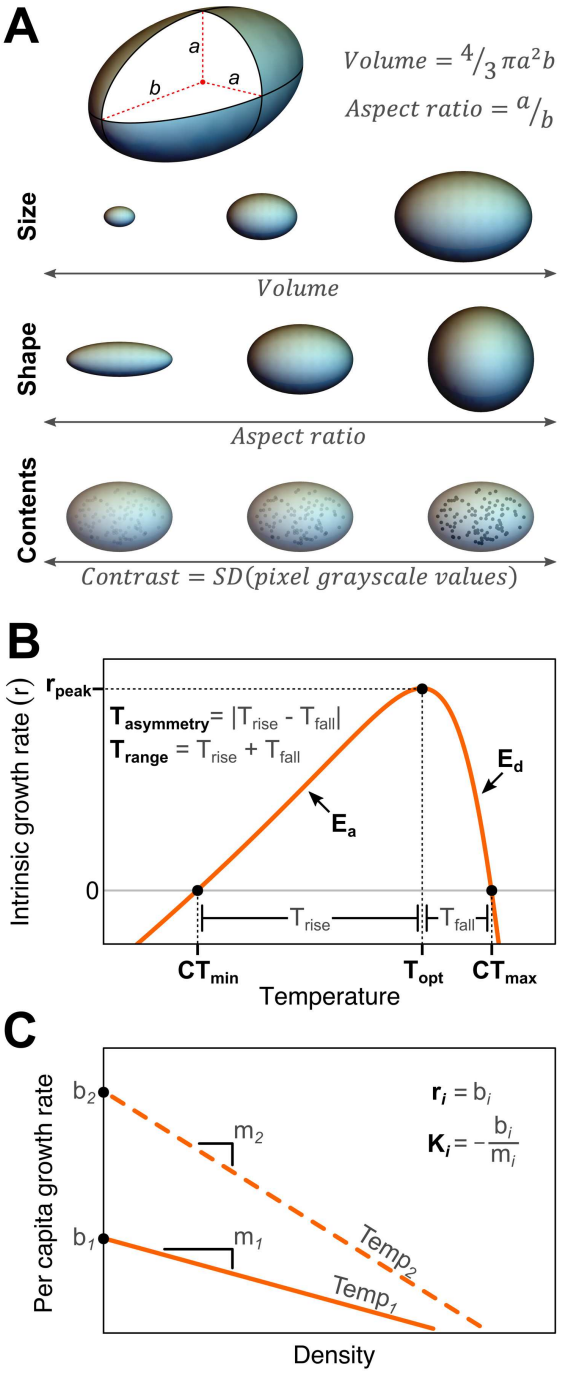

619

620 **Figure 1.** Conceptual diagram demonstrating traits and demographic characteristics of species.

621 (A) Major axes of trait variation in protists can be measured by representing cells as spheroids

622 that vary in size, shape, and contents—which are measured respectively as volume, aspect ratio,

and the standard deviation of pixel grayscale values using flow imaging microscopy. (B) Changes in some aspect of performance (e.g., intrinsic growth rate) in a species across temperatures are captured by the position and shape of a thermal performance curve (TPC). (C) Density dependence in population growth can be evaluated at different temperatures by measuring the y-intercept (b) and slope (s) of the relationship between per-capita growth rate and density.

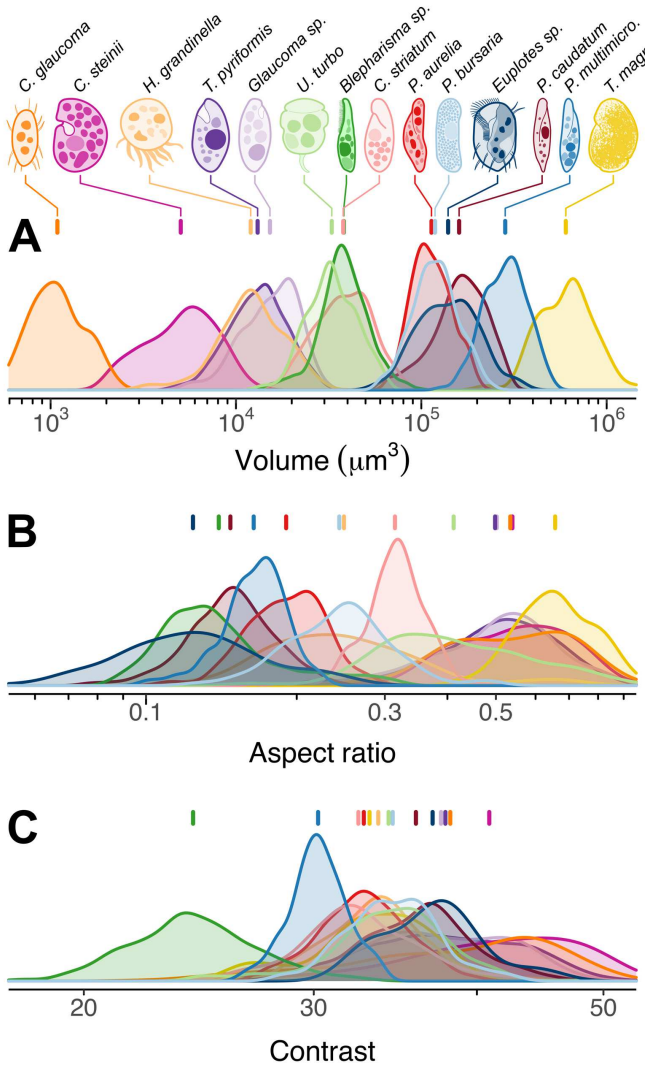

646

647 **Figure 2.** Intra- and inter-specific variation in (A) cell volume (size), (B) cell aspect ratio

648 (shape), and (C) cell contrast (contents) measured for 14 protist species. Bars above each

649 distribution denote mean values.

650

651

652

653

654

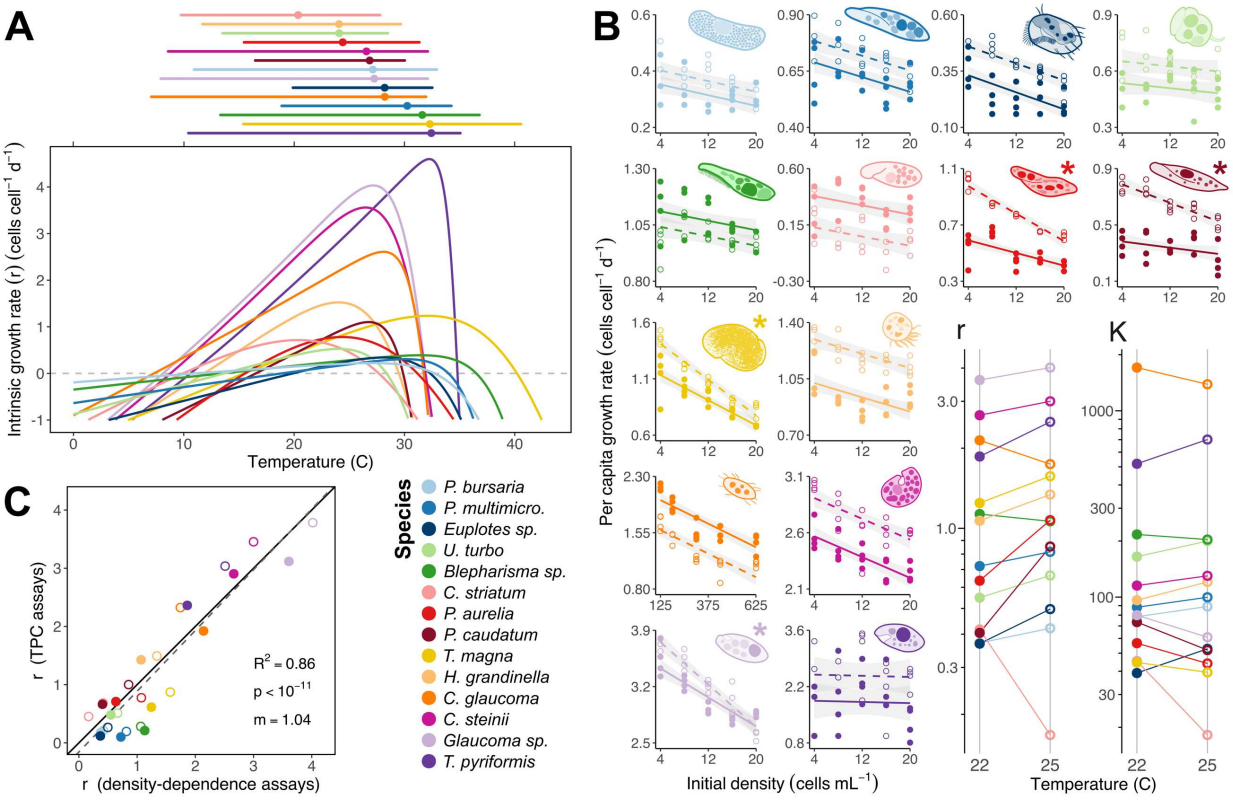

Figure 3. The temperature dependence of population growth measured empirically for 14 protist species. (A) Thermal performance curves (TPCs) with bars (above) showing thermal breadths (T_{range}, where $r > 0$) and points showing thermal optima (T_{opt}). (B) Density dependence of per-capita growth rates measured at two temperatures: 22ºC (solid points/lines) and 25ºC (open points/dashed lines)—lines are significant linear regressions, shaded regions are 95% confidence intervals, and asterisks signify the existence of a significant interaction between density and temperature. *r* and *K* (inset) were calculated from these regressions for each species at each temperature. 'ns' indicates that *K* estimates were not significant for given species. (C) Agreement between *r* estimates from density dependence assays and TPC assays at 22ºC (solid points) and 25ºC (open points).

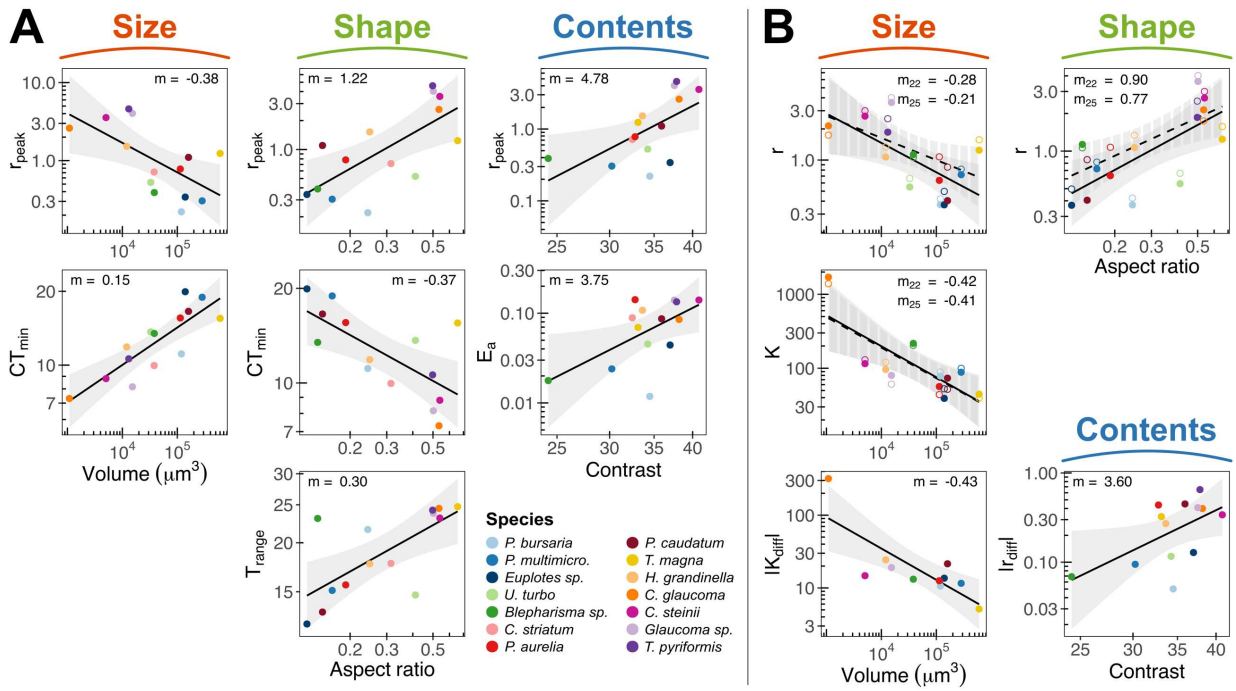

Figure 4. Significant relationships between species mean trait values and (A) TPC parameters and (B) density dependence parameters. Shaded regions are 95% confidence intervals, 'm' indicates the slope of each regression. In (B), solid lines/shading denote 22ºC and dashed lines/shading denote 25ºC.

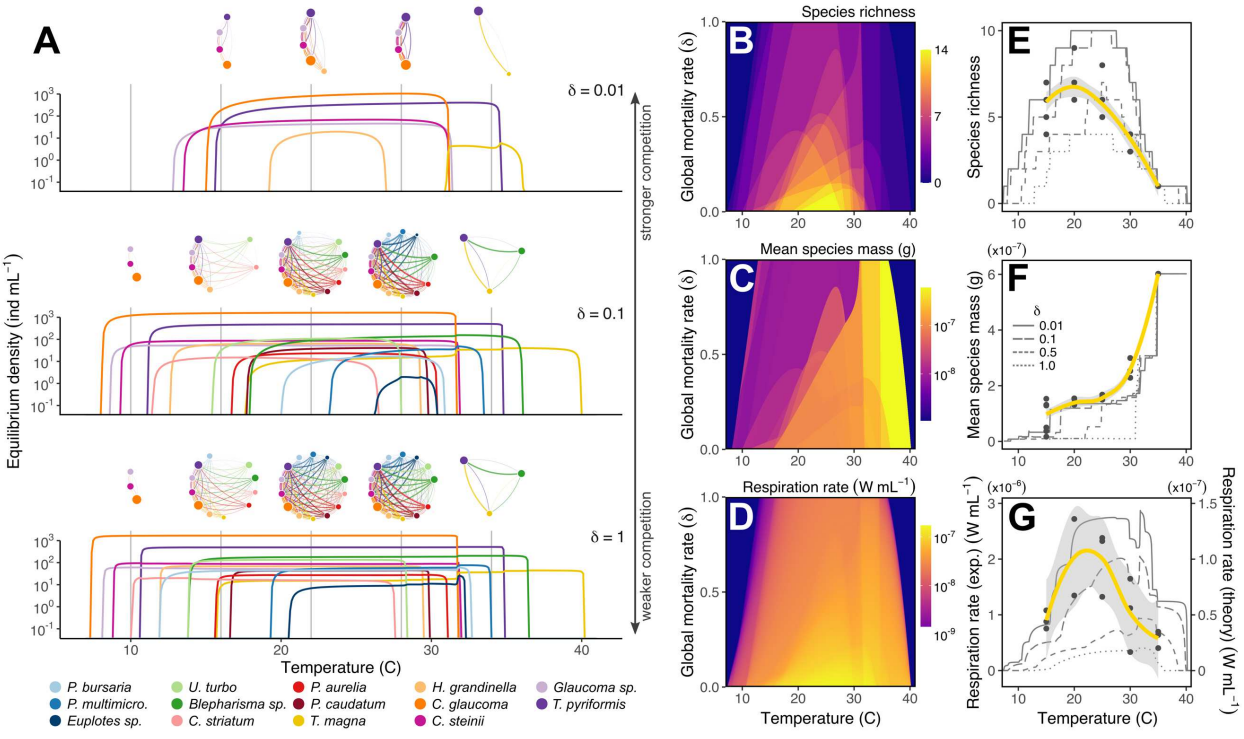

682

683 **Figure 5.** Theoretical (A-D) and experimental (E–G) results for temperature effects on

684 competitive communities. (A) Equilibrium densities across the entire range of viable

685 temperatures for species in this study shown for three different global mortality rates (δ, which

686 controls the strength of competitive differences among species). Network diagrams show

687 community topology and interaction strengths at 10, 16, 22, 28, & 34ºC—node sizes represent

688 equilibrium densities and link weights represent species interaction strengths. Species richness

689 (B & E), mean species mass (C & F), and total community respiration rate (D & G) are shown

690 across a range of temperatures and global mortality rates for theoretical (B–G) and experimental

691 (E–G) communities. For (E-G), yellow lines are nonlinear fits to experimental data (black dots)

692 and gray lines are model predictions for a range of global mortality rates. Note the difference in

693 scales for experimental and theoretical respiration rates in (G), reflecting bacterial respiration in

694 addition to protist respiration in experimental communities.

695

SUPPLEMENTARY MATERIAL

Species	r_{peak}	T_{opt}	CT_{min}	CT_{max}	T_{range}	$TPC_{asymmetry}$	E_a	E_d
Paramecium bursaria	0.22	27.04	11.11	32.73	21.62	10.23	0.01	3.04
Paramecium multimicronucleatum	0.3	30.1	18.92	34.03	15.12	7.26	0.02	4.55
Euplotes sp.	0.34	28.09	19.92	32.33	12.41	3.93	0.04	3.01
Blepharisma sp.	0.39	31.44	13.46	36.54	23.07	12.88	0.02	4.05
Urocentrum turbo	0.53	24.04	13.66	28.38	14.71	6.04	0.05	3.51
Colpidium striatum	0.71	20.38	9.96	27.68	17.72	3.13	0.09	1.27
Paramecium aurelia	0.78	24.36	15.57	31.18	15.62	1.97	0.14	1.21
Paramecium caudatum	1.1	26.76	16.57	29.88	13.31	7.06	0.09	6.13
Tillina magna	1.24	32.12	15.52	40.24	24.72	8.48	0.07	1.92
Halteria grandinella	1.52	24.03	11.86	29.53	17.67	6.66	0.11	2.83
Cyclidium glaucoma	2.61	28.1	7.31	31.78	24.47	17.11	0.09	7.16
Colpoda steinii	3.56	26.47	8.81	31.93	23.12	12.2	0.14	3.88
Glaucoma sp.	4.03	27.17	8.16	31.93	23.77	14.25	0.14	4.96
Tetrahymena pyriformis	4.6	32.25	10.61	34.83	24.22	19.05	0.13	12.3

Table S1. All thermal performance curve (TPC) metrics for each species in this study. Metrics include critical thermal maximum (CT_{max}), critical thermal minimum (CT_{min}), maximum intrinsic growth rate (r_{peak}), activation energy (E_a), deactivation energy (E_d), optimal temperature (T_{opt}), range of viable temperatures (T_{range}), and asymmetry of TPC shape ($TPC_{asymmetry}$).

Species	Best model	Model p-value	Variable	Estimate (β)	Std. Error	p-value
Paramecium bursaria	Main	<0.001	Intercept	0.371	0.020	<0.001
			$N_{initial}$	-0.005	0.001	0.002
			Temperature	0.05	0.016	0.003
Paramecium multimicronucleatum	Main	<0.001	Intercept	0.721	0.030	<0.001
			$N_{initial}$	-0.008	0.002	<0.001
			Temperature	0.095	0.023	<0.001
Euplotes sp.	Main	<0.001	Intercept	0.369	0.024	<0.001
			$N_{initial}$	-0.009	0.002	<0.001
			Temperature	0.128	0.019	<0.001
Urocentrum turbo	Main	0.001	Intercept	0.549	0.039	<0.001
			$N_{initial}$	-0.003	0.003	0.226
			Temperature	0.116	0.030	<0.001
Blepharisma sp.	Main	0.001	Intercept	1.131	0.029	<0.001
			$N_{initial}$	-0.005	0.002	0.015
			Temperature	-0.069	0.023	0.005
Colpidium striatum	Main	<0.001	Intercept	0.417	0.056	<0.001
			$N_{initial}$	-0.009	0.004	0.022
			Temperature	-0.249	0.044	<0.001
Paramecium aurelia	Interaction	<0.001	Intercept	0.636	0.034	<0.001
			$N_{initial}$	-0.011	0.003	<0.001
			Temperature	0.437	0.048	<0.001
			$N_{initial}$*Temp	-0.013	0.004	0.001
Paramecium caudatum	Interaction	<0.001	Intercept	0.405	0.038	<0.001
			$N_{initial}$	-0.006	0.003	0.063
			Temperature	0.449	0.054	<0.001
			$N_{initial}$*Temp	-0.011	0.004	0.011
Tillina magna	Interaction	<0.001	Intercept	1.245	0.043	<0.001
			$N_{initial}$	-0.028	0.003	<0.001
			Temperature	0.324	0.061	<0.001
			$N_{initial}$*Temp	-0.012	0.005	0.015
Halteria grandinella	Main	<0.001	Intercept	1.068	0.034	<0.001
			$N_{initial}$	-0.011	0.002	<0.001
			Temperature	0.271	0.027	<0.001
Cyclidium glaucoma	Main	<0.001	Intercept	2.141	0.057	<0.001
			$N_{initial}$	-0.001	<0.001	<0.001
			Temperature	-0.399	0.049	<0.001
Colpoda steinii	Main	<0.001	Intercept	2.66	0.052	<0.001
			$N_{initial}$	-0.023	0.004	<0.001
			Temperature	0.34	0.041	<0.001
Glaucoma sp.	Interaction	<0.001	Intercept	3.607	0.074	<0.001
			$N_{initial}$	-0.045	0.006	<0.001
			Temperature	0.41	0.104	<0.001
			$N_{initial}$*Temp	-0.021	0.008	0.012
Tetrahymena pyriformis	Main	0.018	Intercept	1.861	0.278	<0.001
			$N_{initial}$	-0.004	0.019	0.854
			Temperature	0.65	0.218	0.005

Table S2. Multiple regression model summaries for the effects of density and temperature on per-capita growth rates for each species. Main effects alone (Main) and main effects +

interaction effect (Interaction) models were significant for all species. Main effects + interaction models were chosen as the 'best model' only when a significant interaction effect existed ($N_{initial}$*Temp), otherwise the main effects model was chosen.

Demographic parameter	R^2	Model p-value	Trait	Estimate (β)	p-value	VIF	U	U%	C	Total
r_{22}	0.643	0.006	Volume	-0.128	0.081	1.274	0.135	20.975	0.296	0.43
			Aspect Ratio	0.161	0.035	1.274	0.213	33.071	0.296	0.508
r_{25}	0.537	0.021	Volume	-0.084	0.234	1.274	0.074	13.858	0.236	0.31
			Aspect Ratio	0.147	0.051	1.274	0.226	42.188	0.236	0.462
r_{peak}	0.661	0.01	Volume	-0.146	0.137	1.335	0.088	13.349	0.317	0.405
			Aspect Ratio	0.176	0.097	1.52	0.114	17.173	0.381	0.495
			Contrast	0.107	0.278	1.419	0.044	6.727	0.316	0.361
CT_{min}	0.811	<0.001	Volume	0.086	0.001	1.274	0.342	42.126	0.357	0.698
			Aspect Ratio	-0.049	0.026	1.274	0.113	13.898	0.357	0.469

Table S3. Commonality analysis to distinguish unique effects of individual traits on demographic parameters. Each row displays a summary of the results of a multiple regression model including the main effects of relevant traits on each demographic parameter (β, standardized by centering and rescaling traits) as well as variance inflation factors (VIF) and the proportion of total R^2 that is unique to each trait (U; shown with percentage of R^2 explained (U%)), common between a given trait and all other traits in the model (C), and the total explained variance based on the unique and common effects of each trait (U + C = Total).

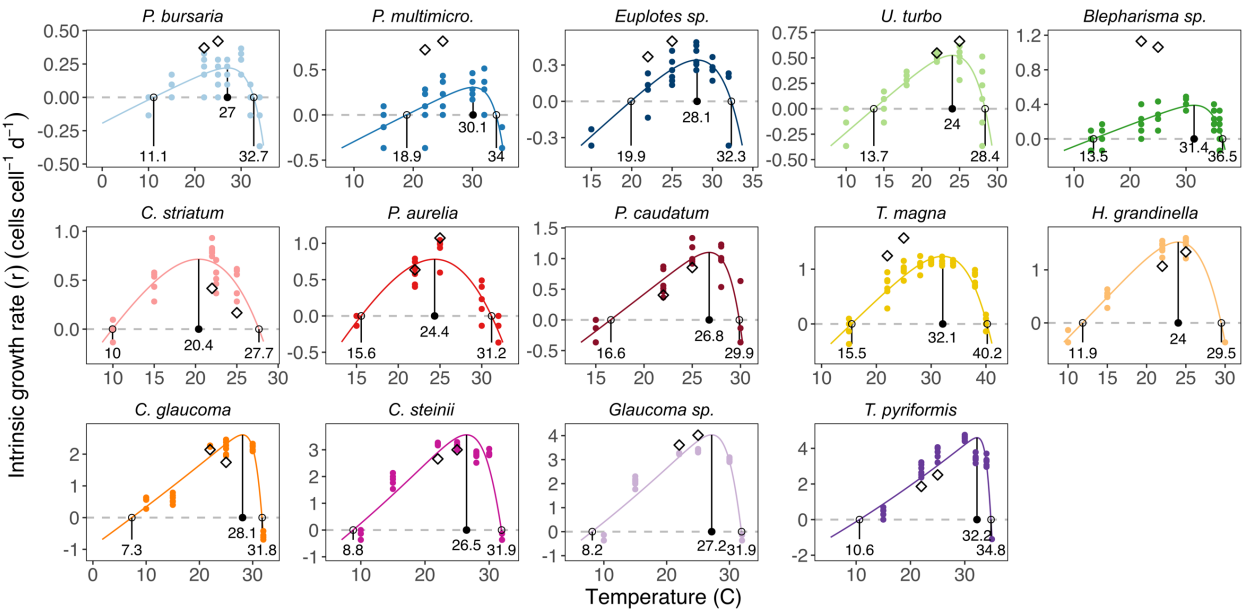

730

731 **Figure S1.** Thermal performance curves (TPCs) for individual species. Colored points are raw

732 data from TPC assays. Open diamonds are r estimates at 22ºC and 25ºC from density dependence

733 assays. Open circles indicate critical thermal minima (CT_{min}) and maxima (CT_{max}) and closed

734 black circles indicate optimal temperatures (T_{opt}).

735

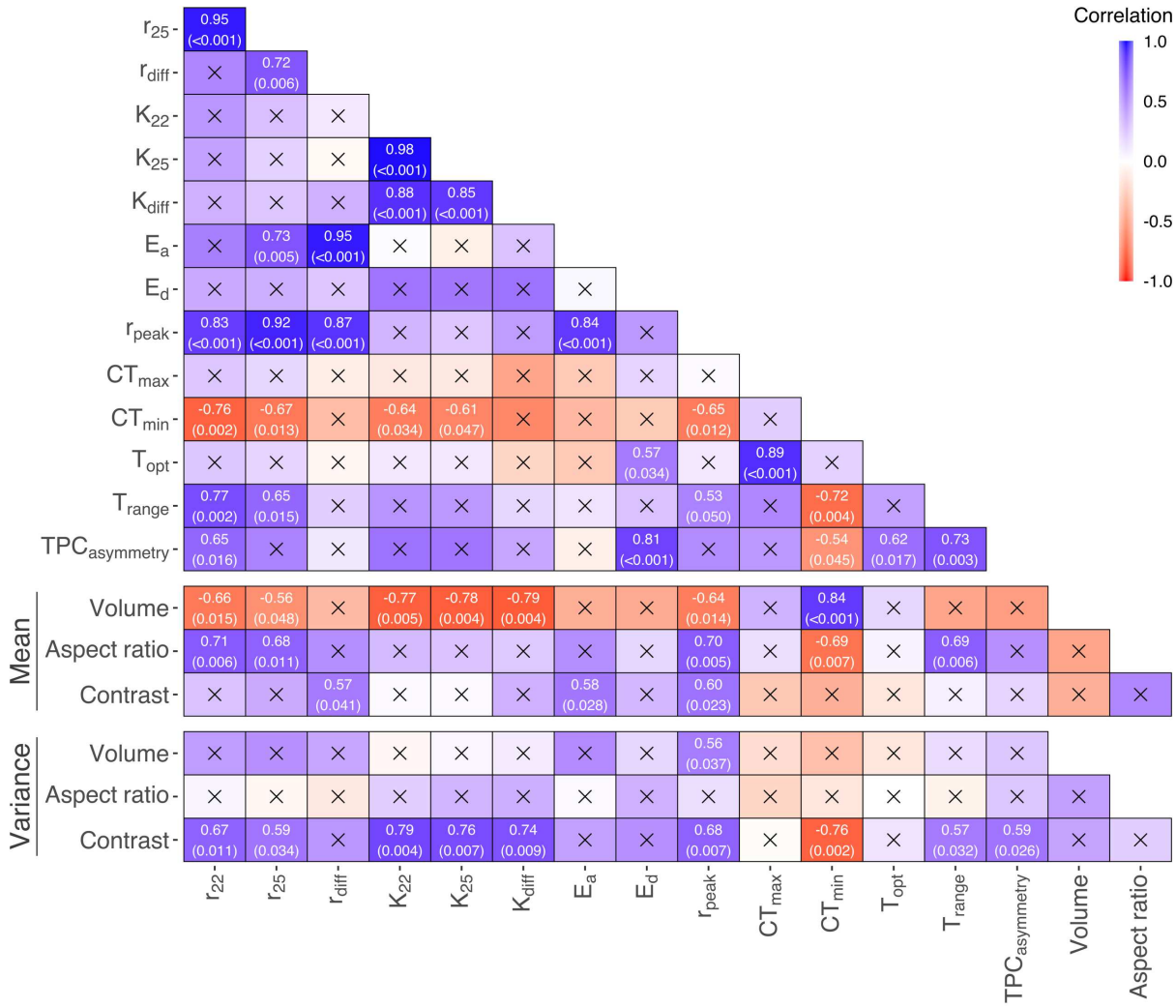

Figure S2. Correlations among demographic parameters and species mean and variance of log-transformed traits (volume, aspect ratio, and contrast). Upper numbers indicate significant correlations, numbers in parentheses indicate p-values, and "X" indicates no significance.

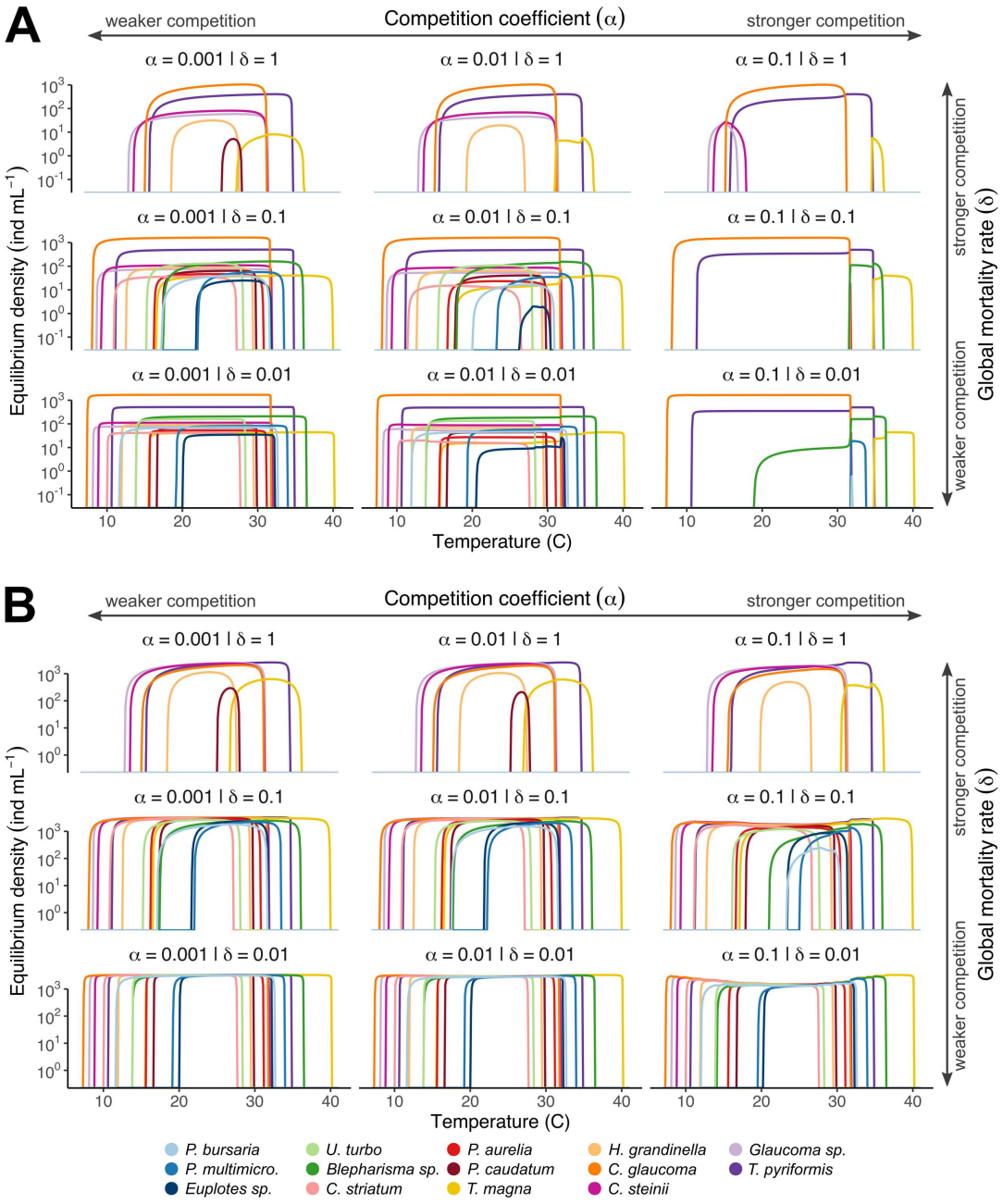

Figure S3. Equilibrium densities for all 14 species across temperatures shown for ranges of interspecific competition coefficients (α) and global mortality rates (δ). In (A), carrying capacities (K_i) for each species i are proportional to empirical carrying capacities as in the main results. In (B), carrying capacities for each species is set to $K = 1$. Thus, the middle column in (A) corresponds to the main results in Figure 5A.

Figures

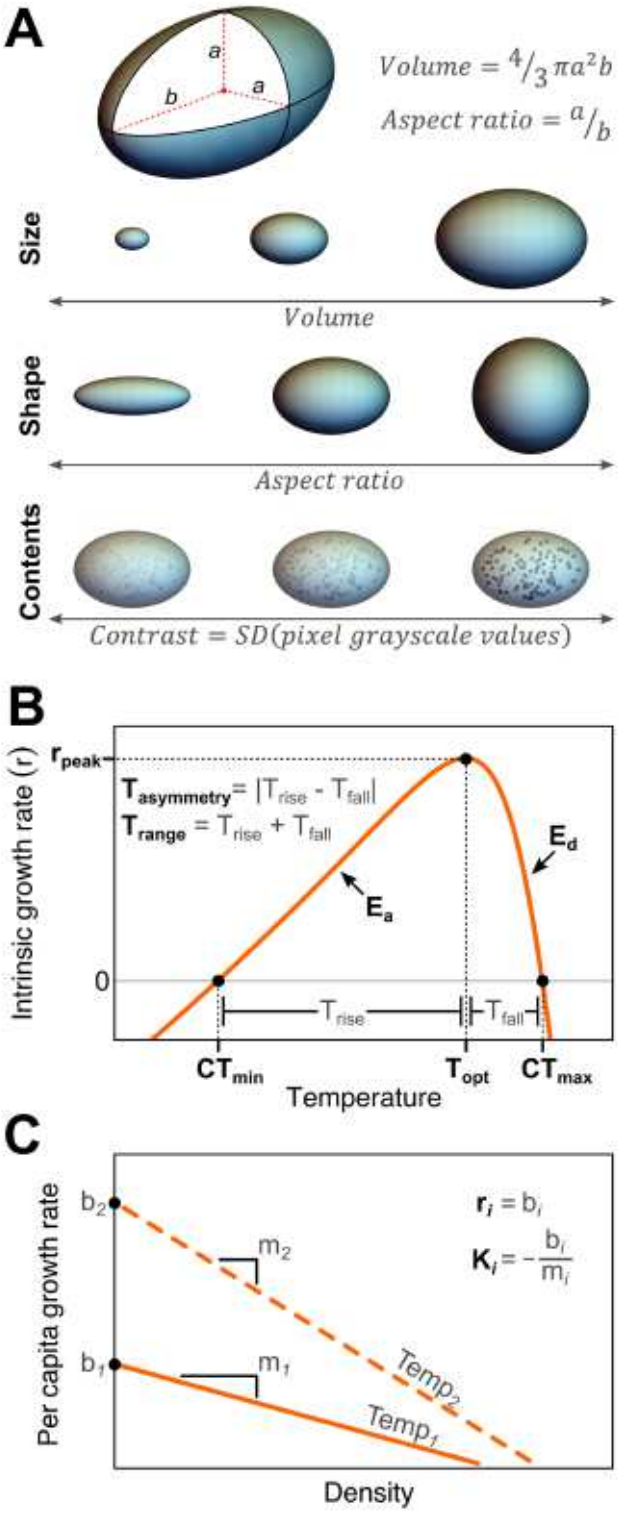

Figure 1

Conceptual diagram demonstrating traits and demographic characteristics of species. (A) Major axes of trait variation in protists can be measured by representing cells as spheroids that vary in size, shape, and contents—which are measured respectively as volume, aspect ratio, and the standard deviation of pixel

grayscale values using flow imaging microscopy. (B) Changes in some aspect of performance (e.g., intrinsic growth rate) in a species across temperatures are captured by the position and shape of a thermal performance curve (TPC). (C) Density dependence in population growth can be evaluated at different temperatures by measuring the y-intercept (b) and slope (s) of the relationship between per-capita growth rate and density.

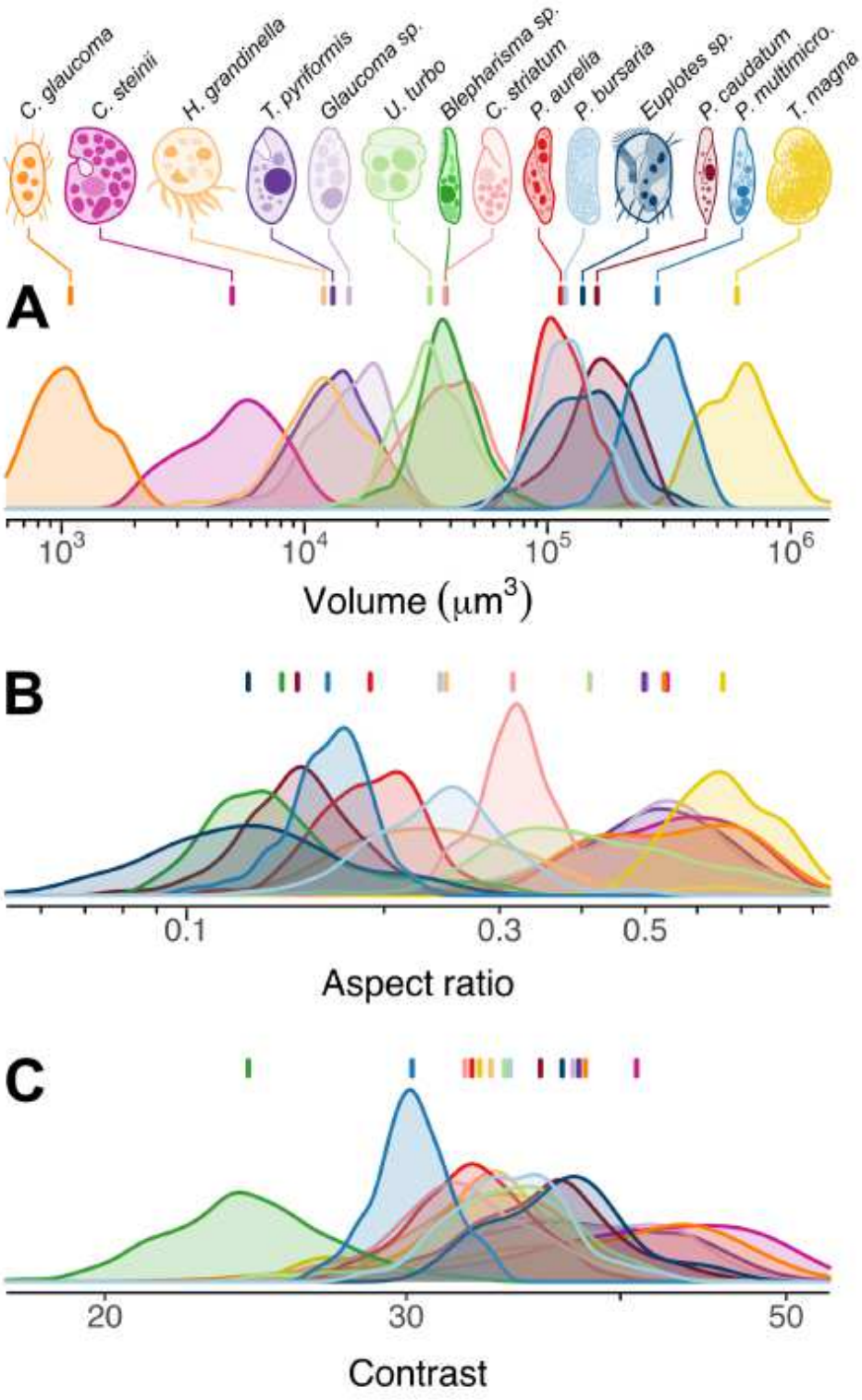

Figure 2

Intra- and inter-specific variation in (A) cell volume (size), (B) cell aspect ratio (shape), and (C) cell contrast (contents) measured for 14 protist species. Bars above each distribution denote mean values.

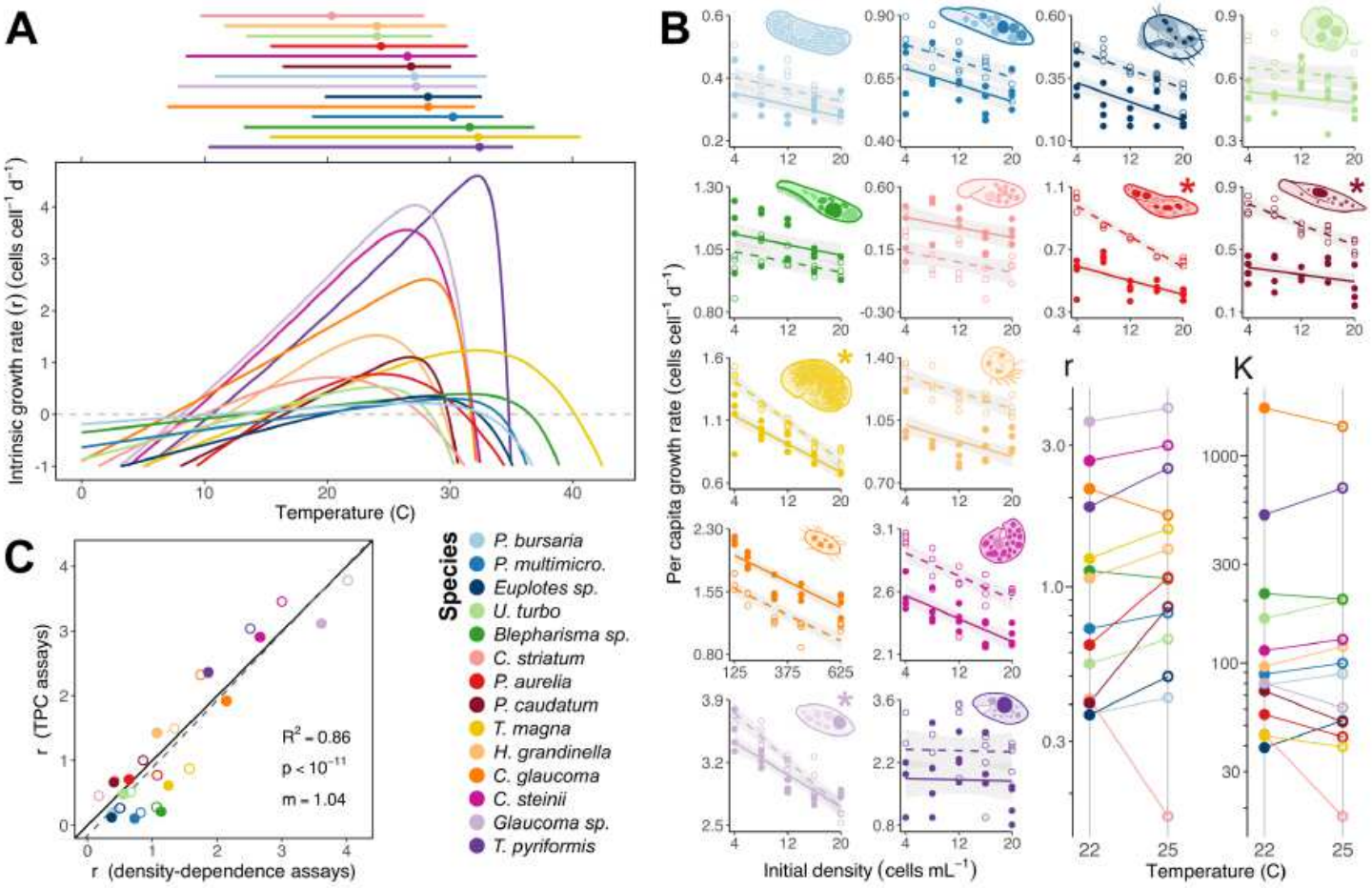

Figure 3

The temperature dependence of population growth measured empirically for 14 protist species. (A) Thermal performance curves (TPCs) with bars (above) showing thermal breadths (Trange, where r > 0) and points showing thermal optima (Topt). (B) Density dependence of per capita growth rates measured at two temperatures: 22ºC (solid points/lines) and 25ºC (open points/dashed lines)—lines are significant linear regressions, shaded regions are 95% confidence intervals, and asterisks signify the existence of a significant interaction between density and temperature. r and K (inset) were calculated from these regressions for each species at each temperature. ‘ns’ indicates that K estimates were not significant for given species. (C) Agreement between r estimates from density dependence assays and TPC assays at 22ºC (solid points) and 25ºC (open points).

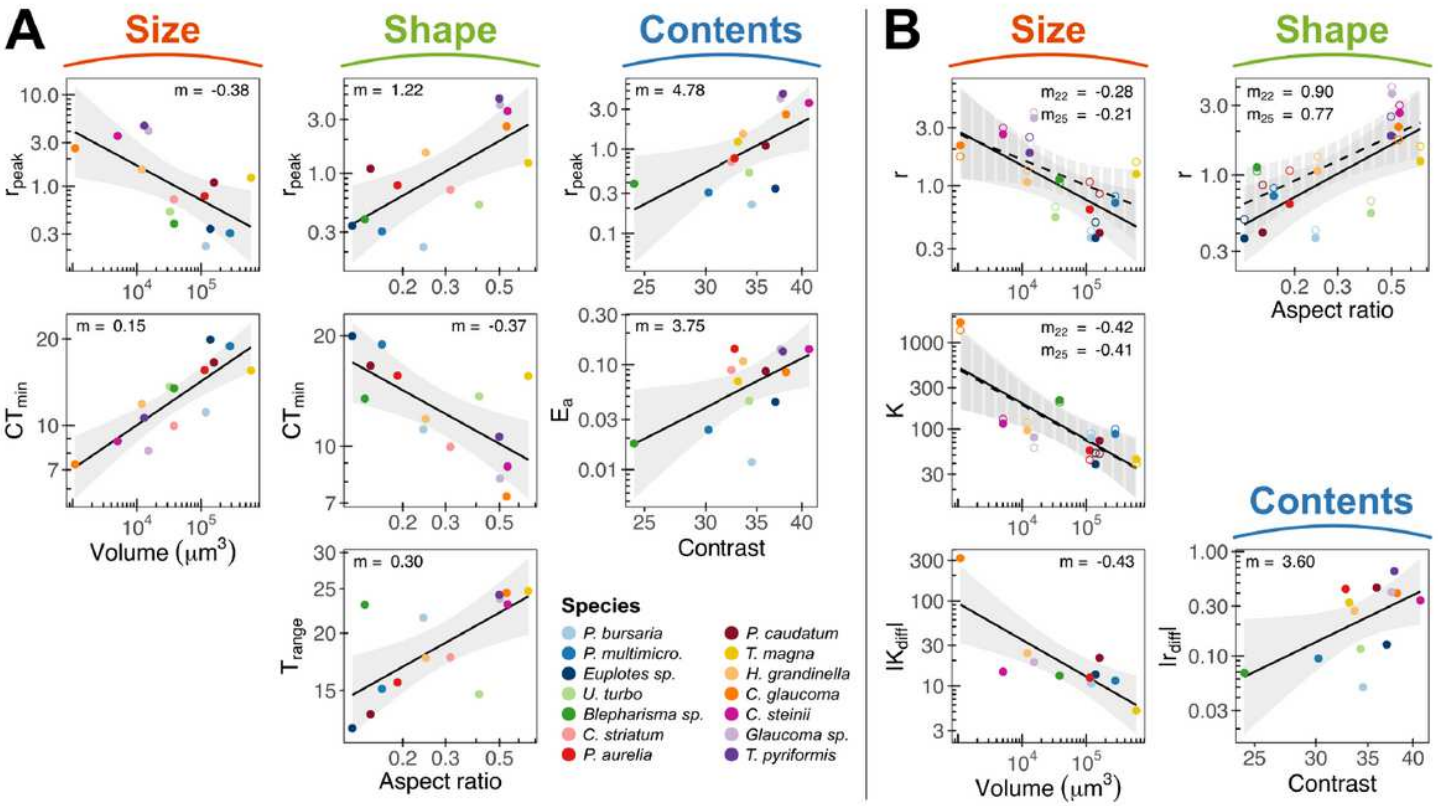

Figure 4

Significant relationships between species mean trait values and (A) TPC parameters and (B) density dependence parameters. Shaded regions are 95% confidence intervals, 'm' indicates the slope of each regression. In (B), solid lines/shading denote 22ºC and dashed lines/shading denote 25ºC.

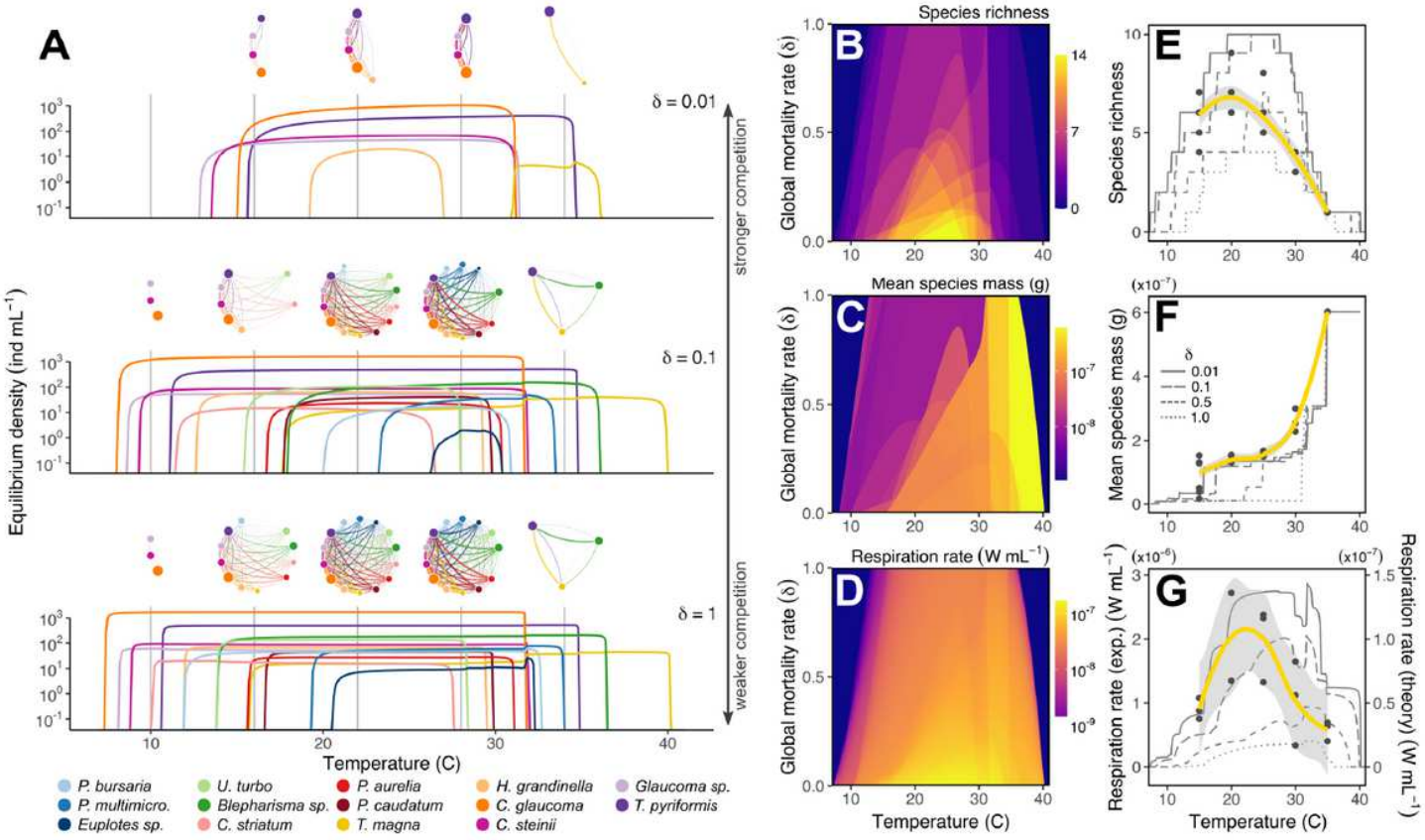

Figure 5

Theoretical (A-D) and experimental (E–G) results for temperature effects on competitive communities. (A) Equilibrium densities across the entire range of viable temperatures for species in this study shown for three different global mortality rates (d, which controls the strength of competitive differences among species). Network diagrams show community topology and interaction strengths at 10, 16, 22, 28, & 34ºC—node sizes represent equilibrium densities and link weights represent species interaction strengths. Species richness (B & E), mean species mass (C & F), and total community respiration rate (D & G) are shown across a range of temperatures and global mortality rates for theoretical (B–G) and experimental (E–G) communities. For (E-G), yellow lines are nonlinear fits to experimental data (black dots) and gray lines are model predictions for a range of global mortality rates. Note the difference in scales for experimental and theoretical respiration rates in (G), reflecting bacterial respiration in addition to protist respiration in experimental communities.